PLOS ONE

RESEARCH ARTICLE

Hydrogen Peroxide Induced Cell Death: The Major Defences Relative Roles and Consequences in *E. coli*

Lionel Uhl, Sam Dukan¤*

Institut de Microbiologie de la Méditerranée – Université Aix-Marseille, Laboratoire de Chimie Bactérienne, CNRS UMR7283, 31 Chemin Joseph Aiguier, 13009 Marseille, France

¤ Current address: Click4Tag SAS, Grand Luminy Technopole, Zone Luminy Entreprise Biotech Case 922, 163 Avenue de Luminy 13288 Marseille Cedex 09 France
* sdukan@imm.cnrs.fr; sam.dukan@click4tag.com

Citation: Uhl L, Dukan S (2016) Hydrogen Peroxide Induced Cell Death: The Major Defences Relative Roles and Consequences in *E. coli*. PLoS ONE 11(8): e0159706. doi:10.1371/journal.pone.0159706

Editor: John Travers Hancock, University of the West of England, UNITED KINGDOM

Received: February 27, 2016

Accepted: July 7, 2016

Published: August 5, 2016

Data Availability Statement: All relevant data are within the paper and its Supporting Information files.

Funding: This work was supported by ANR (Agence National de la Recherchegrant) (ANR-12-BS07-0022 ROSAS). The funders had no role in study design, data collection and analysis, decision to publish, or preparation of the manuscript.

Competing Interests: The authors have declared that no competing interests exist.

Abstract

We recently developed a mathematical model for predicting reactive oxygen species (ROS) concentration and macromolecules oxidation *in vivo*. We constructed such a model using *Escherichia coli* as a model organism and a set of ordinary differential equations. In order to evaluate the major defences relative roles against hydrogen peroxide (H_2O_2), we investigated the relative contributions of the various reactions to the dynamic system and searched for approximate analytical solutions for the explicit expression of changes in H_2O_2 internal or external concentrations. Although the key actors in cell defence are enzymes and membrane, a detailed analysis shows that their involvement depends on the H_2O_2 concentration level. Actually, the impact of the membrane upon the H_2O_2 stress felt by the cell is greater when micromolar H_2O_2 is present (9-fold less H_2O_2 in the cell than out of the cell) than when millimolar H_2O_2 is present (about 2-fold less H_2O_2 in the cell than out of the cell). The ratio between maximal external H_2O_2 and internal H_2O_2 concentration also changes, reducing from 8 to 2 while external H_2O_2 concentration increases from micromolar to millimolar. This non-linear behaviour mainly occurs because of the switch in the predominant scavenger from Ahp (Alkyl Hydroperoxide Reductase) to Cat (catalase). The phenomenon changes the internal H_2O_2 maximal concentration, which surprisingly does not depend on cell density. The external H_2O_2 half-life and the cumulative internal H_2O_2 exposure do depend upon cell density. Based on these analyses and in order to introduce a concept of dose response relationship for H_2O_2-induced cell death, we developed the concepts of "maximal internal H_2O_2 concentration" and "cumulative internal H_2O_2 concentration" (e.g. the total amount of H_2O_2). We predict that cumulative internal H_2O_2 concentration is responsible for the H_2O_2-mediated death of bacterial cells.

Introduction

Oxygen is indisputably essential for life, but it can also impair cell ability to function normally or it can participate in its destruction ([1] and [2]) because of the generation of reactive oxygen species (ROS) like hydrogen peroxide (H_2O_2), superoxide ($O_2^{\bullet -}$) or hydroxyl radical ($HO^{\bullet}$).

In order to better understand ROS dynamic within cells, we recently developed a mathematical model ([3]) for predicting reactive oxygen species (ROS) concentration and macromolecules oxidation *invivo*. This first study principally focuses on $HO^{\bullet}$ dynamic and its consequence on DNA whereas the current study will mainly focus on H_2O_2 dynamic.

Escherichia coli was used as a model organism. In order to build our mathematical model we used data from a large number of articles dealing with enzymes or molecule concentrations (in *E. coli*, kinetic properties and chemical reaction rate constants). We were then able to propose a mathematical model based on a set of ordinary differential equations relating to fundamental principles of mass balance and reaction kinetics. It offers the possibility to simulate properly the experimental results obtained by biologists and therefore to understand the biological parameters involved in the observed phenomena.

The purpose of this study is to use our mathematical model in order to better understand H_2O_2 mode of action on *E. coli* as a model organism.

In aerobic organisms, oxygen oxidizes redox enzymes, generating a flux of H_2O_2 that can potentially damage the cell. For instance, *Escherichia coli* generates about 14 μM H_2O_2 per second when it grows aerobically on glucose ([4]). In order to cope with H_2O_2 stress, microbes typically contain multiple catalases and/or peroxidases. *E. coli* contains one Alkyl hydroperoxide reductase (Ahp) and two different catalases (Cat). Alkyl hydroperoxide reductase is the primary scavenger for endogenous H_2O_2 in *E. coli* ([5]). Catalase contributes little when H_2O_2 levels are low, but it becomes the most effective scavenger when H_2O_2 levels are high ([5]). Moreover, membrane permeability is part of the global defence process against H_2O_2 ([4]). However, to our knowledge, the question of their relative involvement remains unsolved especially with regard to the exogenous H_2O_2 concentration.

Mechanisms involved in H_2O_2 induced cell death were studied by Imlay and Linn ([6] and [7]) who showed that the exposure of *E. coli* to H_2O_2 led to two different modes of killing. The first was observed at low H_2O_2 concentration (1–3 mM H_2O_2) and resulted from the DNA damage caused by $HO^{\bullet}$ ([7]). The second resulted from damage to unknown macromolecules, inflicted more directly, through H_2O_2-mediated oxidation. However, and to our knowledge, the question of the relative involvement of the cumulative or the maximal H_2O_2 dose involvement in this phenomenon remains unsolved. Dose response is a question often raised about radiative hazards. For instance Harrison et al. ([8]) indicated median survival times in rats following intravenous injection of polonium-210. The total alpha-particles-emitted numbers show that the cumulative dose and not the maximal dose is principally responsible for death.

Using our mathematical model, we first investigated the relative role of the different ways (principally Ahp, Cat and membrane) for cells to decrease and fight H_2O_2 oxidative stress. Here we predict that their involvement depends on the H_2O_2 stress level. Moreover and as observed for radiative hazards, we predict that cumulative internal H_2O_2 concentration is responsible for the H_2O_2-mediated death of bacterial cells.

Materials and Methods

The model assumes that all molecule concentrations are homogeneous in cells. We therefore describe the problem with a dynamic system of ordinary differential equations (ODE) instead of using a complex algorithm such as the Next-Sub-Volume Method. Indeed, one algorithm

generally used to study the compartmentalization of molecules in microorganisms (for instance *E. coli*) is the Next-Sub-volume Method. It is a Gillespie-like ([9] and [10]) method approaching the spatial effects of diffusive phenomena and chemical reaction. According to the Next Sub-volume Method, the side length ℓ of the square sub-volumes has to satisfy the two inequalities

$$R \ll \ell \text{ and } \tau_{diff} = \frac{\ell^2}{6D} \ll \tau_{react}$$

where R is the larger radius of a molecule of substrat

and D the diffusion constant of H_2O_2

τ_{diff} represents the characteristic time of diffusion

τ_{react} represents the characteristic time of reaction

The first inequality indicates that dissociation events can be properly defined within sub-volumes. The second criterion specifies that the time for any molecule to leave a sub-volume is much smaller than the shortest reaction time τ_{min} among the molecular species, so that all molecules are homogeneously distributed within the sub-volumes. For example, the 3D simulations are typically performed with $\ell = 0,1\ \mu$m and the depth $h = \ell$ of the sub-volumes, which is many times larger than the average radius of a substrat even protein. Considering the H_2O_2 molecule maximal number, the reaction initially follows a pseudo-first order kinetic with rate constant $k' = k[H_2O_2]$ and the characteristic time of reaction is therefore $\tau = 1/k'$. This time has to be compared to the characteristic time of diffusion of H_2O_2: $\tau_{diff} = \frac{\ell^2}{6D} \approx 10^{-6}$ s (with H_2O_2 diffusion constant $D = 2\ 10^{-9}\ m^2.s^{-1}$). This comparison gives $\tau = 1/k' = 1/k[H_2O_2] \gg 10^{-6}$ or $[H_2O_2] \ll 10^6/k$. Even with very high rate constant such as $10^6\ M^{-1}s^{-1}$, the inequality imposes $[H_2O_2] \ll 1$ M. In conclusion, while $[H_2O_2] \ll 1$ M, the diffusion within the cell is faster than the reaction rate and we do not need to consider compartmentalization.

$O_2^{\bullet-}$ and H_2O_2 are involved in many reactions. Of course we do not take all possible reactions into account, for instance, we do not consider the Haber-Weiss reaction, because our simulations showed no change with or without its consideration and moreover because the relevance of this reaction *in vivo* is questionable ([11] and [12]); actually adding the Haber-Weiss reaction, numerical simulations show that it is negligible whether H_2O_2 concentration is under 0.1 mol·L^{-1}. Using published rate constants, we propose here some simplifications and approximations of the system achieved by neglecting the kinetically non-significant reaction. $HO^{\bullet}$ was studied in a previous article ([3]).

Superoxide kinetics

$O_2^{\bullet-}$ is mainly involved in the following kinetically significant reactions:

Its production:

$$metabolism\ production \xrightarrow{k_1} O_2^{\bullet-}$$

Its dismutation by SOD (superoxide dismutase)

$$O_2^{\bullet-} + H^+ \xrightarrow[SOD]{k_2} \frac{1}{2}H_2O_2 + \frac{1}{2}O_2$$

These two reactions lead to the following ordinary differential equation (ODE) coming from

the balance between production and dismutation by SOD:

$$\frac{\mathrm{d}[O_2^{\bullet -}]}{\mathrm{d}t} = k_1 - k_2[SOD][O_2^{\bullet -}]$$

Internal hydrogen peroxide kinetics

H_2O_2 appears significantly in the following reactions: Its productions:

$$metabolism\ production \xrightarrow{k_1'} H_2O_2$$

$$O_2^{\bullet -} + H^+ \xrightarrow[SOD]{k_2} \frac{1}{2}H_2O_2 + \frac{1}{2}O_2$$

Its dismutation by catalase (Cat) or Alkylhydroperoxidase (Ahp)

$$H_2O_2 \xrightarrow{Cat} H_2O + \frac{1}{2}O_2$$

$$H_2O_2 \xrightarrow{Ahp} H_2O + \frac{1}{2}O_2$$

Its diffusion across cell membrane

$$H_2O_2 \xrightarrow{k_{diff}} H_2O_{2out}$$

k_{diff} has been calculated using the membrane permeability coefficient ($P = 1.6 \times 10^{-3}$ cm/s), the membrane surface area ($A = 1.41 \times 10^{-7}$ cm^2) and cell volume ($V = 3.2 \times 10^{-15}$ L) given by Seaver and Imlay ([4]), therefore $k_{diff} = \frac{P \times S}{V}$.

The ODE becomes:

$$\begin{aligned}\frac{\mathrm{d}[H_2O_2]}{\mathrm{d}t} &= k_1' \\ &\quad + \frac{1}{2}k_2[SOD][O_2^{\bullet -}] \\ &\quad - \frac{k_{cat}^{Ahp}[Ahp][H_2O_2]}{[H_2O_2] + K_M^{Ahp}} - \frac{k_{cat}^{Kat}[Cat][H_2O_2]}{[H_2O_2] + K_M^{Kat}} \\ &\quad - k_{diff}([H_2O_2] - [H_2O_2]_{out})\end{aligned}$$

where H_2O_{2out} corresponds to H_2O_2 in the external habitat of the cell.

K_M (K_M^{Kat} for catalase and K_M^{Ahp} for alkylhydroperoxidase) is the Michaelis constant. k_{cat} (k_{cat}^{Kat} for catalase and k_{cat}^{Ahp} for alkylhydroperoxidase) is the turnover number, it represents the maximum number of molecules (here H_2O_2) that an enzyme is able to convert into products per second.

External hydrogen peroxide

$$\frac{\mathrm{d}[H_2O_2]_{out}}{\mathrm{d}t} = k_{diff}\frac{n \cdot V_{in}}{V_{out} - nV_{in}}\left([H_2O_2] - [H_2O_2]_{out}\right)$$

The cell density is given by n. V_{in} represents the cell internal volume and V_{out} corresponds to

the total volume. Of course, as microorganisms cannot take up more space than their medium, we have the inequality $V_{out} - nV_{in} \gg 0$.

Cell density

For under 10 minutes experimental time (consistent with most of our simulation), cell density could be considered as a constant but for long time simulation we propose the logistic equation for cell growing function. The logistic equation (also called the Verhulst model) is a model of population growth first published by Pierre Verhulst ([13] and [14]). The continuous version of the Verhulst model is described by the following differential equation:

$$\frac{\mathrm{d}n}{\mathrm{d}t} = r \cdot n\left(1 - \frac{n}{n_{max}}\right)$$

where r is the Malthusian parameter (rate of population growth) and n_{max} the maximum sustainable population. This differential equation gives an analytical solution:

$$n(t) = \frac{n_0 e^{rt}}{1 + \frac{n_0}{n_{max}}\left(e^{rt} - 1\right)}$$

where n_0 is the initial density. This value depends on the experiment. We choose carrying capacity $n_{max} = 5 \times 10^9$ cell/mL. The maximal rate of growth usually shows that a growing bacterial population doubles at regular intervals near a characteristic time $\tau_d \approx 20$ minutes. Therefore $n(t)$ expression also gives:

$$n(t) = \frac{n_0 2^{t/\tau_d}}{1 + \frac{n_0}{n_{max}}\left(2^{t/\tau_d} - 1\right)}$$

where $r = \ln(2)/\tau_d$.

Nevertheless this characteristic time depends on cell history and stress. For example, even 0.2 mM of H_2O_2 when added to a logarithmically growing *E. coli* population is enough to generate an immediate decrease in the number of viable cells. This phenomenon is transient and the original number of viable cells is recovered only about 40 minutes after the occurrence of the sub-lethal stress ([15]). This transient phenomenon is mirrored at the population level by a lag phase in which optical density remains almost constant for about 40 minutes. A fraction dies, and then the remaining bacteria resume growth so that the number of viable cells reaches the original number. For instance Chang et al. ([16]) also report a lag phase of about 40 minutes after an addition of 1.5 mM of H_2O_2. In order to take into account this phenomenon we consider that $\tau_d \to \infty$ if $t < 40$ minutes so that $n(t < 40\ min) = constant$ after H_2O_2 oxidative stress.

We were not concerned with stationary phase because no experiment carried out in this work reached the maximum sustainable population.

Kinetic constants

The kinetic constants used in this work are gathered in Table 1 according to Imlay and Fridovich ([17]) and Seaver and Imlay ([5] and [4]).

Numerical simulations

All numerical simulations were carried out using the MATLAB ODE solver ode15s for stiff differential equations. The multistep solver ode15s is a variable order solver based on the numerical differentiation formulas.

Table 1. Kinetic constants used to describe H_2O_2 evolution.

Kinetic constants	
k_1	5.7×10^{-6} mol·L^{-1}·s^{-1}
$k_2[SOD]$	2.8×10^{4} s^{-1}
k_2	1.5×10^{9} mol^{-1}·L·s^{-1}
V_{in}	3.2×10^{-15} L
k'_1	12×10^{-6} mol·L^{-1}·s^{-1}
$k_{cat}^{Ahp}[Ahp]$	6.6×10^{-4} mol·L^{-1}·s^{-1}
K_M^{Ahp}	1.2×10^{-6} mol·L^{-1}
$k_{cat}^{Kat}[Cat]$	4.9×10^{-1} mol·L^{-1}·s^{-1}
K_M^{Kat}	5.9×10^{-3} mol·L^{-1}
k_{diff}	70 s^{-1}

doi:10.1371/journal.pone.0159706.t001

Results and Discussion

This section presents the analytical study of the dynamic system. This analysis will provide us with insight into the kinetic parameters significantly important for the dynamics of *ROS*.

Internal hydrogen peroxide

Without exogenous stress. In the wild-type strain, $O_2^{\bullet-}$ equilibrium is rapidly reached. Indeed the characteristic time of $O_2^{\bullet-}$ evolution is $1/k_2[SOD] \approx 35\mu$s. Therefore we can consider $O_2^{\bullet-}$ as a constant and we can assume that $[O_2^{\bullet-}](t) \approx [O_2^{\bullet-}]_\infty$ (S1 File supporting information data for demonstration).

So in terms of changes to internal H_2O_2 concentration, we approach

$k'_1 + {}^1\!/_2 k_2[SOD][O_2^{\bullet-}] \approx k'_1 + {}^1\!/_2 k_1$ because $[O_2^{\bullet-}] \approx [O_2^{\bullet-}]_\infty$ Let us call $k'_1 + {}^1\!/_2 k_1 = k_{prod}$.

That is a first point, $O_2^{\bullet-}$ dismutation by SOD involved nearly an increase of 25% in the endogenous H_2O_2 production.

Moreover, in the absence of exogenous H_2O_2, we can consider that:

$$[H_2O_2] \ll K_M^{Ahp}, K_M^{Cat}$$

so the differential equation system can be simplified to a linear system:

$$\frac{\mathrm{d}[H_2O_2]}{\mathrm{d}t} = k_{prod} - \left(\frac{k_{cat}^{Ahp}[Ahp]}{K_M^{Ahp}} + \frac{k_{cat}^{Kat}[Cat]}{K_M^{Kat}}\right)[H_2O_2] - k_{diff}\left([H_2O_2] - [H_2O_2]_{out}\right)$$

$$\frac{\mathrm{d}[H_2O_2]_{out}}{\mathrm{d}t} = k'_{diff}\left([H_2O_2] - [H_2O_2]_{out}\right)$$

with:

$$k'_{diff} = k_{diff}\frac{n \cdot V_{in}}{V_{out} - nV_{in}}$$

Let us call $\frac{k_{cat}^{Ahp}[Ahp]}{K_M^{Ahp}} + \frac{k_{cat}^{Kat}[Cat]}{K_M^{Kat}} = k_{enz}$, then the differential equation system can be written with a

matrix structure:

$$\frac{\mathrm{d}}{\mathrm{d}t}\begin{pmatrix}[H_2O_2]\\ [H_2O_2]_{out}\end{pmatrix}=\begin{pmatrix}k_{prod}\\ 0\end{pmatrix}+\begin{pmatrix}-(k_{enz}+k_{diff}) & k_{diff}\\ k'_{diff} & -k'_{diff}\end{pmatrix}\begin{pmatrix}[H_2O_2]\\ [H_2O_2]_{out}\end{pmatrix}$$

The matrix eigenvalues are $\lambda_1 > \lambda_2$:

$$\lambda_1=\frac{-(k_{enz}+k_{diff}+k'_{diff})+\sqrt{(k_{enz}+k_{diff}+k'_{diff})^2-4k_{enz}k'_{diff}}}{2}<0$$

$$\lambda_2=\frac{-(k_{enz}+k_{diff}+k'_{diff})-\sqrt{(k_{enz}+k_{diff}+k'_{diff})^2-4k_{enz}k'_{diff}}}{2}<0$$

According to the value of the reaction rate constant, we can make the following approximation: $\lambda_1 \approx -\frac{k_{enz}}{(k_{enz}+k_{diff})}k'_{diff}$ and $\lambda_2 \approx -(k_{enz}+k_{diff})$.

The full matrix V with columns corresponding to the eigenvectors is:

$$V=\begin{pmatrix}k'_{diff}+\lambda_1 & k'_{diff}+\lambda_1\\ k'_{diff} & k'_{diff}\end{pmatrix}$$

The system becomes $\begin{pmatrix}[H_2O_2]\\ [H_2O_2]_{out}\end{pmatrix}=V\begin{pmatrix}Ae^{\lambda_1 t} & 0\\ 0 & Be^{\lambda_2 t}\end{pmatrix}$

The resolution shows a bi-exponential expression:

$$[H_2O_2]=\left(k'_{diff}+\lambda_1\right)Ae^{\lambda_1 t}+\left(k'_{diff}+\lambda_2\right)Be^{\lambda_2 t}+\frac{k_{prod}}{k_{enz}} \quad (1)$$

$$[H_2O_2]_{out}=k'_{diff}Ae^{\lambda_1 t}+k'_{diff}Be^{\lambda_2 t}+\frac{k_{prod}}{k_{enz}} \quad (2)$$

with

$$A=\frac{\left([H_2O_2]_0-\frac{k_{prod}}{k_{enz}}\right)k'_{diff}-\left([H_2O_2]_{out0}-\frac{k_{prod}}{k_{enz}}\right)\left(k'_{diff}+\lambda_2\right)}{(\lambda_1-\lambda_2)k'_{diff}} \quad (3)$$

$$B=\frac{\left([H_2O_2]_0-\frac{k_{prod}}{k_{enz}}\right)k'_{diff}-\left([H_2O_2]_{out0}-\frac{k_{prod}}{k_{enz}}\right)\left(k'_{diff}+\lambda_1\right)}{(\lambda_2-\lambda_1)k'_{diff}} \quad (4)$$

In this first approach, $[H_2O_2]_0 = 0$ and $[H_2O_2]_{out0} = 0$: initial concentrations are taken to be zero.

From the very beginning, $[H_2O_2] \approx \left(k'_{diff}+\lambda_1\right)A+\left(k'_{diff}+\lambda_2\right)Be^{\lambda_2 t}+\frac{k_{prod}}{k_{enz}}$ as $e^{\lambda_1 t} \approx 1$ because $|\lambda_1| \approx 0$.

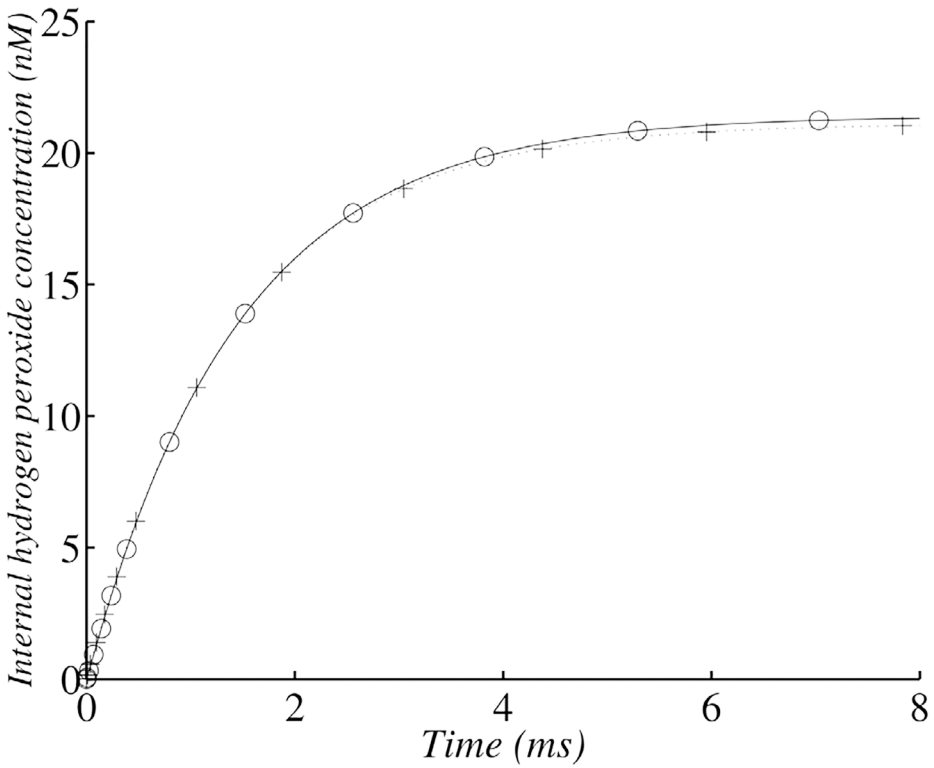

Fig 1. Changes in internal H_2O_2 concentration in the wild-type strain with 10^7 cells ml^{-1}. (+) corresponds to the analytical solution of internal H_2O_2 evolution according to the simplified system and (○)) corresponds to the whole model solved with numerical methods.

doi:10.1371/journal.pone.0159706.g001

Therefore $A \approx -\frac{k_{prod}}{k_{enz}k'_{diff}}$ and $B = \frac{k_{prod}}{(k_{enz}+k_{diff})^2}$

$$k'_{diff} + \lambda_1 = k'_{diff} - \frac{k_{enz}}{(k_{enz}+k_{diff})}k'_{diff} = \frac{k_{diff}}{(k_{enz}+k_{diff})}k'_{diff};$$

$$k'_{diff} + \lambda_2 \approx -(k_{enz}+k_{diff});$$

In conclusion: $[H_2O_2] \approx \frac{k_{prod}}{k_{enz}+k_{diff}}(1-e^{-(k_{enz}+k_{diff})t})$

The first plateau (in Fig 1) corresponds to the compromise between production and consumption, but consumption now also depends on diffusion across cell membrane. Indeed, the value of this first plateau is approximately $\frac{k_{prod}}{k_{enz}+k_{diff}}$.

The numerical values are ([4]):

$$k_{enz} = 633\,\mathrm{s}^{-1} \text{ with } \frac{k_{cat}^{Ahp}[Ahp]}{K_M^{Ahp}} = 550\,\mathrm{s}^{-1}; \frac{k_{cat}^{Kat}[Cat]}{K_M^{Kat}} = 83\,\mathrm{s}^{-1}; k_{diff} = 70\,\mathrm{s}^{-1}$$

These values indicate that diffusion across the cell membrane accounts for approximately 10% of the H_2O_2 eliminated, a level of activity close to that of Cat activity (≈12%). As previously reported ([5]), Ahp was identified as the principal scavenger (≈78%).

The first plateau concentration for H_2O_2 is therefore $\frac{k_{prod}}{k_{enz}+k_{diff}} \approx 21$ nM.

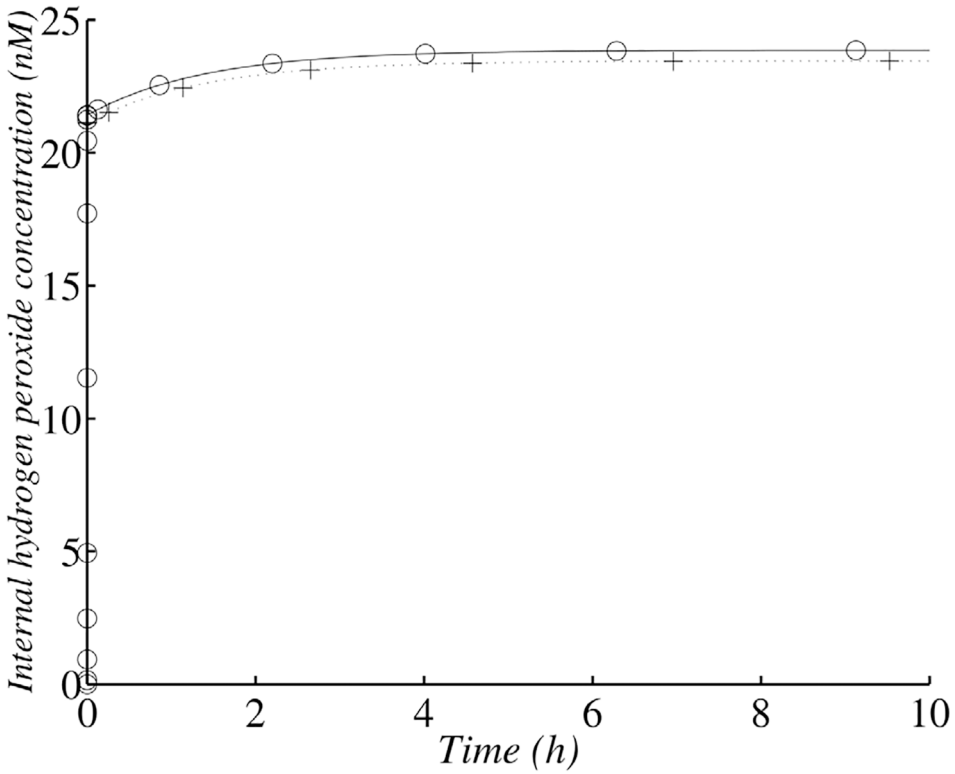

Fig 2. Changes in internal H_2O_2 concentration in the wild-type strain with 10^6 cells ml^{-1}. (+) corresponds to the analytical solution according to the simplified system and (○)) corresponds to the whole model and a numerical solution.

doi:10.1371/journal.pone.0159706.g002

For instance, in an Ahp(-) mutant without Cat induction, this concentration would be $\frac{k_{prod}}{\frac{k_{cat}^{Kat}[Cat]}{K_M^{Kat}}+k_{diff}} \approx 97$ nM.

After this transition step, we had $e^{\lambda_2 t} \approx 0$. The change in H_2O_2 concentration therefore follows this equation:

$$[H_2O_2] = \frac{k_{prod}}{k_{enz}} - \frac{k_{prod}}{k_{enz}} \frac{k_{diff}}{(k_{enz} + k_{diff})} e^{\lambda_1 t}$$

This second step is slower and depends on the number of cells, with the final steady-state concentration of H_2O_2 reached more rapidly for denser cell populations (Figs 2 and 3).

The final steady-state value is $[H_2O_2]_\infty = \frac{k_{prod}}{k_{enz}} \approx 23.5$ nM and is not dependent on cell number. This value is close to that obtained by numerical simulation (23.9 nM) and to that proposed by Imlay (20 nM) ([4]).

For instance, in an Ahp(-) mutant without Cat induction, this value would be $\frac{k_{prod} K_M^{Kat}}{k_{cat}^{Kat}[Cat]} \approx 179$ nM (identical to the numerical simulation value and close to the value of 100 nM proposed by Seaver and Imlay ([4]).

This second step in the change in H_2O_2 concentration depends on $\lambda_1 \approx -\frac{k_{enz}}{(k_{enz}+k_{diff})} k'_{diff}$, which depends on cell concentration *via* the k'_{diff}.

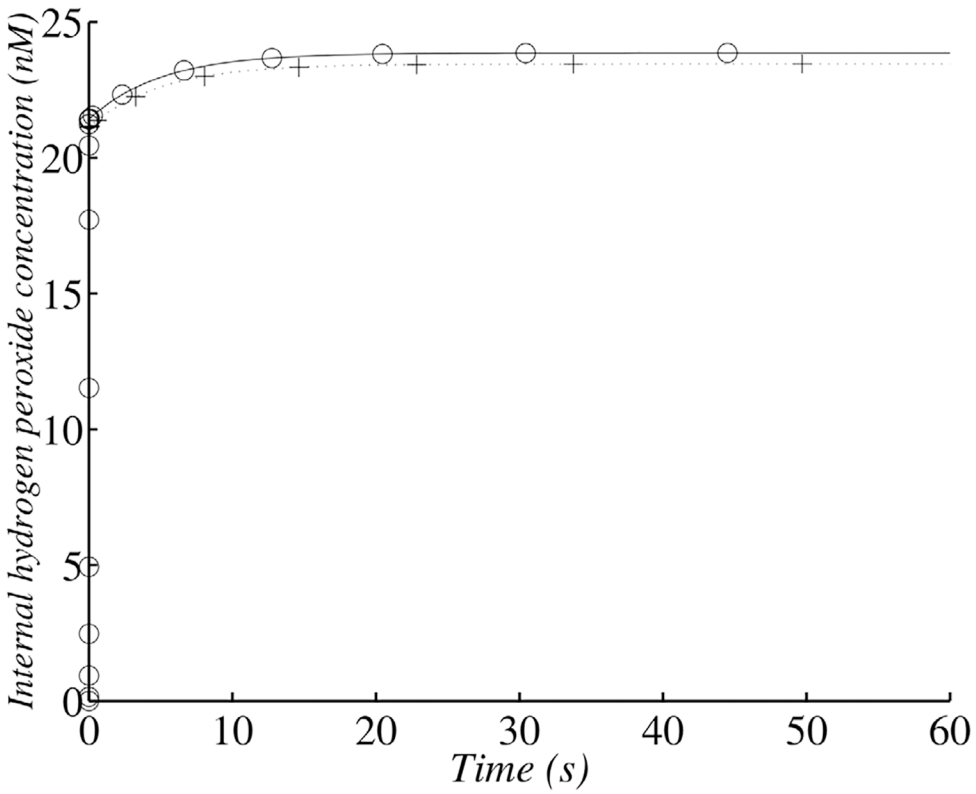

Fig 3. Changes in H_2O_2 concentration in the wild-type strain with 10^9 cells ml^{-1}. (+) corresponds to the analytical solution according to the simplified system and (○)) corresponds to the whole model and a numerical solution.

doi:10.1371/journal.pone.0159706.g003

The results are summarized in Table 2.

With exogenous stress. We propose linear approximations of Michaelis-Menten kinetics. Internal H_2O_2 concentration approximately follows the law outlined below. Let us consider an experiment involving the addition of exogenous H_2O_2. The initial *ROS* concentrations in the cell are taken to be the steady-state values obtained without exogenous H_2O_2. The system requires modification as follows:

$$\begin{aligned}\frac{\mathrm{d}[H_2O_2]}{\mathrm{d}t} &= k_1' + {}^1\!/_2\ k_2[SOD][O_2^{\bullet -}] \\ &\quad - \frac{k_{cat}^{Ahp}[Ahp][H_2O_2]}{[H_2O_2] + K_M^{Ahp}} - \frac{k_{cat}^{Kat}[Cat][H_2O_2]}{[H_2O_2] + K_M^{Kat}} \\ &\quad - k_{diff}([H_2O_2] - [H_2O_2]_{out}) \\ \frac{\mathrm{d}[H_2O_2]_{out}}{\mathrm{d}t} &= k_{diff}\frac{n \cdot V_{in}}{V_{out} - nV_{in}}\left([H_2O_2] - [H_2O_2]_{out}\right)\end{aligned}$$

As the system is nonlinear there is no analytical solution so with a view to solving the system, we had to compare the value obtained for the internal concentration of H_2O_2 with the K_M values of Ahp and Cat to simplify the Michaelis-Menten expression. Moreover, cell behavior (and thus the dynamic system) depends on the comparison of internal H_2O_2 concentration

Table 2. H_2O_2 steady-state concentration.

$[H_2O_2]$ (nmol L^{-1})	In this work	Seaver, Imlay [4]
Wild type	24	21
HPI+ HPII+ Ahp- (*AhpCF*[(a)])	179	100
HPI- HPII- Ahp+ (*KatEKatG*)	28	23

At steady state, the internal concentration is shown for cells in LB at 37°C.
(a) without induced HPI levels.

doi:10.1371/journal.pone.0159706.t002

with the K_M values of Ahp and Cat. This comparison is essential to simplify the system into a linear one, which will then be solvable. This kind of study is frequently carried out and provides useful insight into the workings of systems. For example, Polynikis *et al.* ([18]) compared different modeling approaches (complete nonlinear model, simplified piecewise linear model etc.) for gene regulatory networks using Hill functions, a general form of the Michaelis-Menten equation.

To approximate the Michaelis-Menten hyperbole into a piecewise linear function, let us first examine the contribution of the two enzymes.

The rate (see Fig 4) followed the same pattern of change as that presented by Seaver and Imlay ([5]). Ahp was the leading scavenger in conditions of 17 μM exogenous H_2O_2 (see intersection point in Fig 5).

We can consider that, in the presence of less than 10 μM H_2O_2, Ahp activity is linear (Fig 5) and that Cat activity is linear at concentrations below 10 mM (due to its K_M value). At H_2O_2 concentrations of more than 30 μM, Ahp activity is saturated.

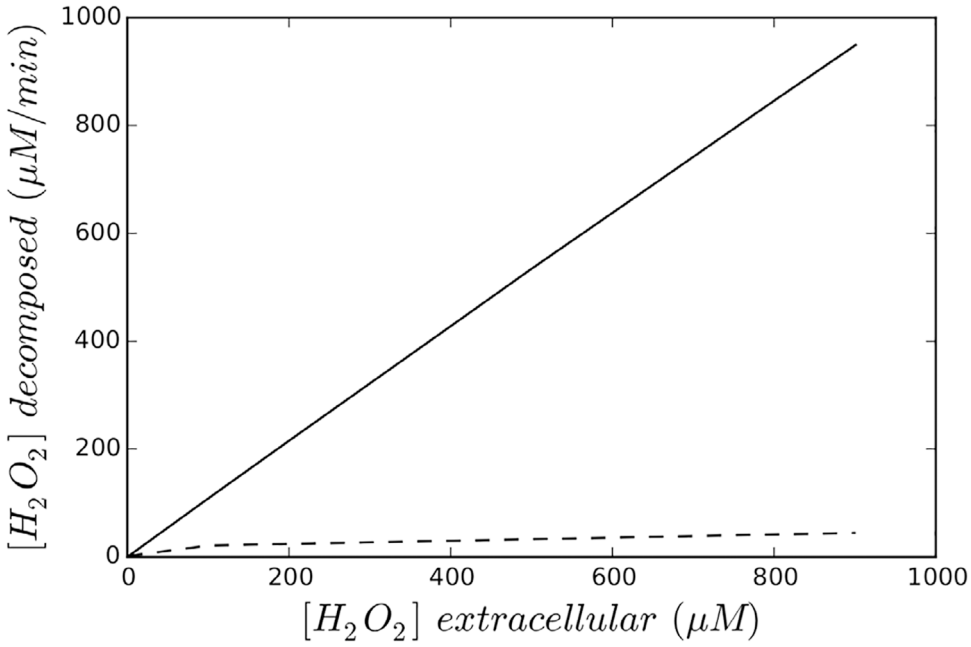

Fig 4. Kinetics of exogenous H_2O_2 decomposition for 1.5×10^8 *E. coli* cells ml^{-1}. The dotted line corresponds to the Cat(-) mutant and solid line corresponds to the Ahp (-) mutant.

doi:10.1371/journal.pone.0159706.g004

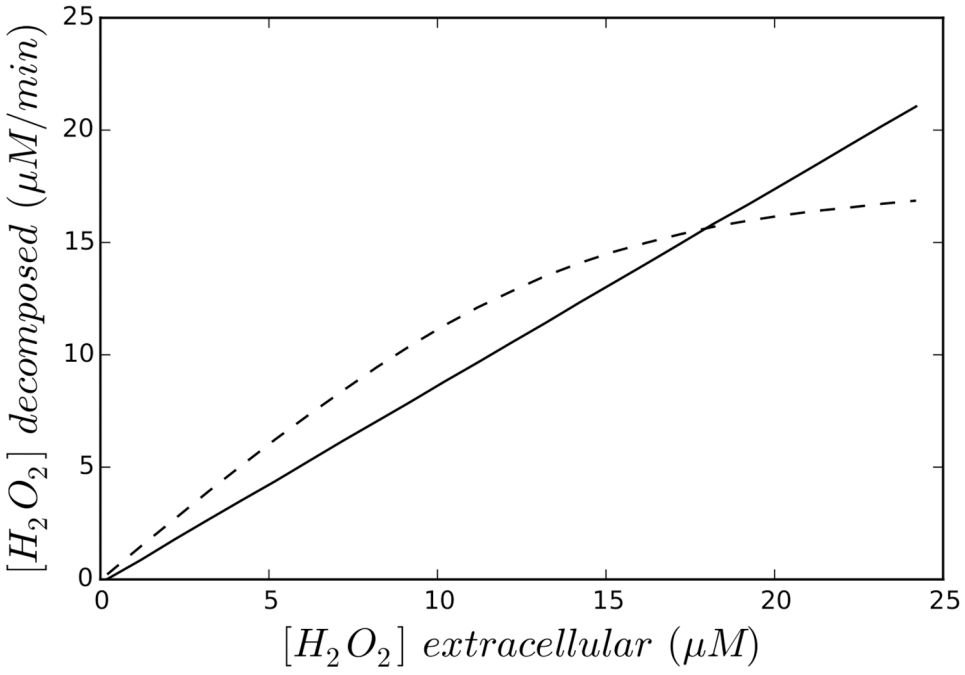

Fig 5. Kinetics of exogenous H_2O_2 decomposition for 1.5×10^8 *E. coli* cells ml^{-1}. The dotted line corresponds to the Cat(-) mutant and solid line corresponds to the Ahp (-) mutant (higher magnification for Fig 4).

doi:10.1371/journal.pone.0159706.g005

According to the Michaelis-Menten equation, we should consider Ahp activity to be linear when $[H_2O_2] \ll K_M^{Ahp} \approx 1\ \mu$M, but linearity was observed when $[H_2O_2]_{out} < 10\ \mu$M. It is unclear why there is a difference of one order of magnitude between exogenous $[H_2O_2]_{out}$ and internal $[H_2O_2]$ at the limit of linearity.

Such a difference was reported in another experiment presented by Seaver and Imlay ([4]) while studying H_2O_2 fluxes.

In this experiment, whole cells seemed to scavenge H_2O_2 less efficiently than cell extracts. The cell membrane slows the entry of H_2O_2, resulting in lower rates of decomposition. It also protects cells against high H_2O_2 concentrations, by decreasing the maximum value of H_2O_2 concentration. This phenomenon is described in more detail below. The simulation (Fig 6) for extract was modeled by eliminating membrane diffusion and the metabolism associated with *ROS* production. There is a perfect match between numerical simulation and the experimental results of Seaver and Imlay.

Two situations can be distinguished based on these previous observations.

In the first case, $[H_2O_2] \ll K_M^{Ahp}$ corresponds to $[H_2O_2]_{out} < 10\ \mu$M and to $[H_2O_2] \ll K_M^{Cat}$. The system approaches Michaelis-Menten terms as follows:

$$\begin{aligned} \frac{k_{cat}^{Ahp}[Ahp][H_2O_2]}{[H_2O_2]+K_M^{Ahp}} + \frac{k_{cat}^{Kat}[Cat][H_2O_2]}{[H_2O_2]+K_M^{Kat}} &\approx \frac{k_{cat}^{Ahp}[Ahp]}{K_M^{Ahp}} + \frac{k_{cat}^{Kat}[Cat]}{K_M^{Kat}}[H_2O_2] \\ &= k_{enz}[H_2O_2] \end{aligned}$$

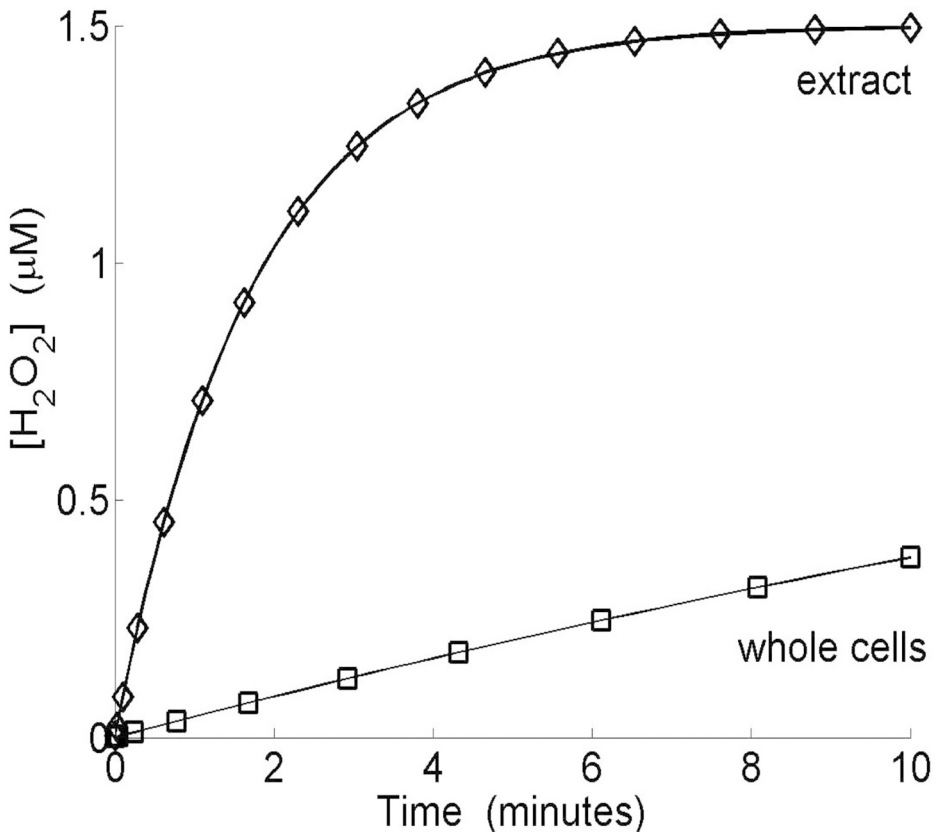

Fig 6. *In silico*, breakdown of exogenous H_2O_2 by whole cells (Ahp(-) mutant) or cell extract. Simulation runs with 4×10^6 cells ml^{-1}. Moreover, Seaver and Imlay ([5]) observed that an Ahp(-) mutant contained seven times as much total Cat as wild-type cells. We therefore used the same ratio.

doi:10.1371/journal.pone.0159706.g006

In the second case, if $[H_2O_2] \gg K_M^{Ahp}$, corresponding to $[H_2O_2]_{out} > 30\ \mu$M and to $[H_2O_2] \ll K_M^{Cat}$, then the system approaches Michaelis-Menten terms as follows:

$$\begin{aligned} \frac{k_{cat}^{Ahp}[Ahp][H_2O_2]}{[H_2O_2]+K_M^{Ahp}} + \frac{k_{cat}^{Kat}[Cat][H_2O_2]}{[H_2O_2]+K_M^{Kat}} &\approx \left(k_{cat}^{Ahp}[Ahp] + \frac{k_{cat}^{Kat}[Cat]}{K_M^{Kat}}\right)[H_2O_2] \\ &= k_{cat}^{Ahp}[Ahp] + k'_{enz}[H_2O_2] \end{aligned}$$

where $\frac{k_{cat}^{Kat}[Cat]}{K_M^{Kat}} = k'_{enz}$.

Then we examine Ahp activity with a micromolar exogenous H_2O_2 concentration. In the first case ($[H_2O_2] \ll K_M^{Ahp}$ and $[H_2O_2] \ll K_M^{Cat}$), the differential equation system appears to be the same as that without exogenous H_2O_2, but $[H_2O_2]_{out} \neq 0$. As $[H_2O_2]_0 = \frac{k_{prod}}{k_{enz}}$, the constants A and B can be simplified as follows:

$$A = \frac{-\left([H_2O_2]_{out0} - \frac{k_{prod}}{k_{enz}}\right)(k'_{diff} + \lambda_2)}{(\lambda_1 - \lambda_2)k'_{diff}}$$

and

$$B = \frac{-\left([H_2O_2]_{out0} - \frac{k_{prod}}{k_{enz}}\right)\left(k'_{diff} + \lambda_1\right)}{(\lambda_2 - \lambda_1)k'_{diff}}$$

Moreover as $\lambda_1 \approx -\frac{k_{enz}}{(k_{enz}+k_{diff})}k'_{diff}$ and $\lambda_2 \approx -(k_{enz} + k_{diff})$ with $|\lambda_1| << |\lambda_2|$ and $|k'_{diff}| << |\lambda_2|$

$$(k'_{diff} + \lambda_1)A \approx -(k'_{diff} + \lambda_2)$$

$$B \approx \left([H_2O_2]_{out0} - \frac{k_{prod}}{k_{enz}}\right)\frac{k_{diff}}{k_{diff} + k_{enz}}$$

therefore:

$$[H_2O_2] = \left([H_2O_2]_{out0} - \frac{k_{prod}}{k_{enz}}\right)\frac{k_{diff}}{k_{diff} + k_{enz}}\left(e^{\lambda_1 t} - e^{\lambda_2 t}\right) + \frac{k_{prod}}{k_{enz}}$$

This bi-exponential function shows that changes in internal H_2O_2 concentration follow two phases. There is a first phase, with a large rate constant $-\lambda_2 \approx k_{enz} + k_{diff}$ corresponding to the scavenging process, followed by a much slower second phase, with a low rate constant $-\lambda_1 > 0$ corresponding to the diffusion from the external H_2O_2 into the cell. This second phase is faster for larger numbers of cells because k'_{diff} is highly dependent on cell concentration.

$-\lambda_1 \approx \frac{k_{enz}}{(k_{enz}+k_{diff})}k'_{diff}$ and as $k_{enz} \gg k_{diff}$ we can approach $-\lambda_1 \approx k'_{diff}$.

This function therefore reaches a maximum as $\frac{d[H_2O_2]}{dt} = 0$ for:

$$t_{\max} = \frac{1}{\lambda_2 - \lambda_1}\ln\left(\frac{\lambda_1}{\lambda_2}\right) \approx \frac{1}{(k_{enz} + k_{diff})}\ln\left(\frac{(k_{enz} + k_{diff})^2}{k_{enz}k'_{diff}}\right)$$

This time is weakly dependent on cell numbers. For example, $t_{\max} \approx 18$ ms with 10^7 cells ml^{-1} and 11 ms with 10^9 cells ml^{-1}.

The maximum internal H_2O_2 concentration is approximately:

$$[H_2O_2]_{\max} \approx \left([H_2O_2]_{out0} - \frac{k_{prod}}{k_{enz}}\right)\frac{k_{diff}}{k_{diff} + k_{enz}} + \frac{k_{prod}}{k_{enz}}$$

and as $[H_2O_2]_{out0} \gg \frac{k_{prod}}{k_{enz}} = [H_2O_2]_{\infty}$ which can be approached by:

$$[H_2O_2]_{\max} \approx \frac{k_{diff}[H_2O_2]_{out0}}{k_{diff} + k_{enz}}$$

therefore

$$\frac{[H_2O_2]_{\max}}{[H_2O_2]_{out0}} \approx \frac{1}{1 + k_{enz}/k_{diff}} \approx \frac{1}{9}$$

The balance between the elimination processes in the value of the maximal internal H_2O_2

concentration is due to:

$$\frac{k_{cat}^{Ahp}[Ahp]}{K_M^{Ahp}(k_{enz}+k_{diff})} \approx 78\% \text{ to Ahp}$$

$$\frac{k_{cat}^{Kat}[Cat]}{K_M^{Kat}(k_{enz}+k_{diff})} \approx 12\% \text{ to Cat}$$

and

$$\frac{k_{diff}}{k_{enz}+k_{diff}} \approx 10\%$$

to elimination by diffusion throughout cell membrane

The maximal value of internal H_2O_2 concentration is almost one tenth the initial exogenous H_2O_2 concentration. This phenomenon reflects the role of the cell membrane in limiting diffusion. The need to diffuse across the cell membrane limits the influx of exogenous H_2O_2 and this process is highly effective at low exogenous H_2O_2 concentrations. The difference of one order of magnitude between exogenous $[H_2O_2]_{out}$ and internal $[H_2O_2]$ arises because the membrane creates a rate-limiting step.

To illustrate this, we will investigate cell behaviour in the presence of 1.5 μM exogenous H_2O_2.

After its peak value (Fig 7), internal H_2O_2 concentration decreases because of scavenging, but diffusion across cell membrane is the process which limits the rate of H_2O_2 disappearance, therefore H_2O_2 decrease is slow. The membrane creates a rate-limiting step.

The maximal value is the approximate value of the first plateau proposed by Gonzalez-Flecha and Demple ([19]). It corresponds to the ratio of the rate of H_2O_2 influx by diffusion to levels of scavenging and elimination by diffusion.

The experiments of Seaver and Imlay ([5]) showed that even non-induced cells scavenged micromolar concentrations of exogenous H_2O_2 very quickly. For example, in a culture corresponding to 0.1 OD_{680} unit (corresponding to around 1.5×10^7 cells ml^{-1}), they found that the half time of H_2O_2 in the medium was only 3.5 minutes, and that in a culture of 1.0 OD unit it was 20 s.

The exogenous H_2O_2 concentration approximately follows the law outlined below:

$$[H_2O_2]_{out} = \left([H_2O_2]_0 - \frac{k_{prod}}{k_{enz}}\right)e^{\lambda_1 t} + \frac{k_{prod}}{k_{enz}}$$

where

$$\lambda_1 \approx -\frac{k_{enz}}{(k_{enz}+k_{diff})}k'_{diff} \approx k'_{diff}$$

Its exponential decrease depends on the k'_{diff} rate constant, which is strongly dependent on cell numbers. The half-life of H_2O_2 in the medium is approximately $t_{1/2} \approx \frac{\ln 2}{k'_{diff}}$ and is a decreasing function of cell number. So, with an OD_{680} of 0.1 (Fig 8) we find that $t_{1/2} \approx 210$ s (3.5 min) and with an OD_{680} of 1 we find that $t_{1/2} \approx 21$ s (Fig 9). A comparison of the experimental data and the analytical results indicates that our model describes the change in H_2O_2 correctly.

Finally we examine Ahp activitys, with a high H_2O_2 concentration. In the second case, when $[H_2O_2] \gg K_M^{Ahp}$, corresponding to $[H_2O_2]_{out} > 30$ μM, the differential equation system can be

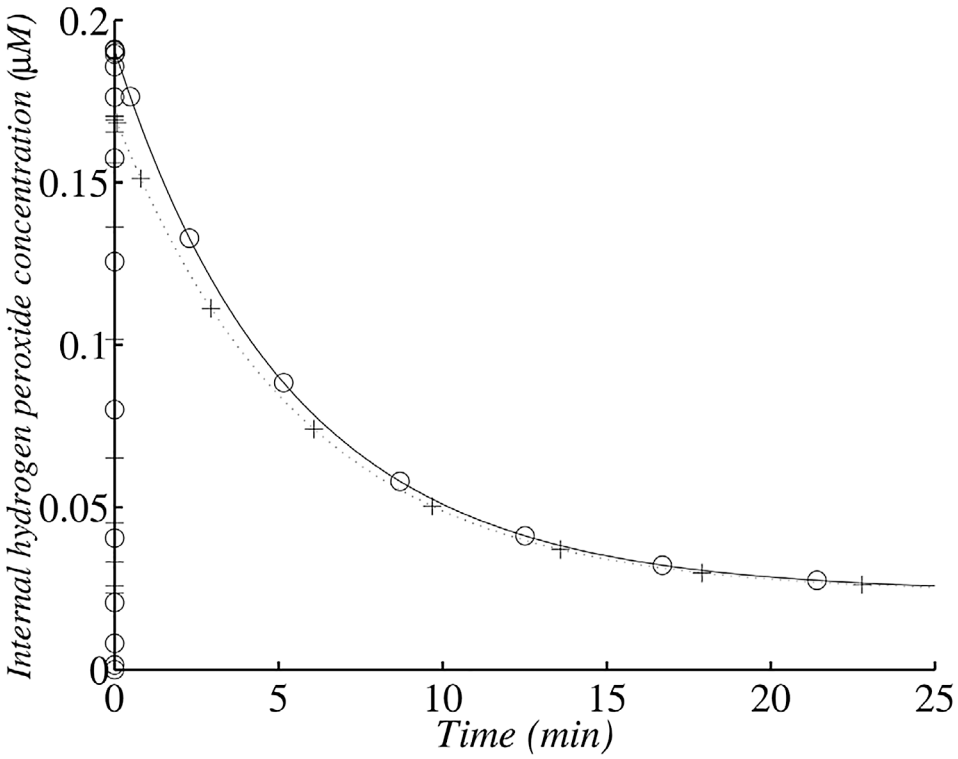

Fig 7. Changes in internal H_2O_2 concentration in the wild type after the addition of 1.5 μM exogenous H_2O_2 with 1.45×10^7 cells ml^{-1}. (+) corresponds to the analytical solution according to the simplified system and (○) corresponds to the numerical solution of the whole model. The simulation was run with 1.45×10^7 cells ml^{-1} (corresponding to an OD_{600} value of 0.1).

doi:10.1371/journal.pone.0159706.g007

written with a matrix structure:

$$\frac{\mathrm{d}}{\mathrm{d}t}\begin{pmatrix}[H_2O_2]\\ [H_2O_2]_{out}\end{pmatrix} = \begin{pmatrix}k'_{prod}\\ 0\end{pmatrix} + \begin{pmatrix}-(k'_{enz}+k_{diff}) & k_{diff}\\ k'_{diff} & -k'_{diff}\end{pmatrix}\begin{pmatrix}[H_2O_2]\\ [H_2O_2]_{out}\end{pmatrix}$$

where $k'_{prod} = k'_1 + {}^1\!/_2 k_1 - k^{Ahp}_{cat}[Ahp]$ is the usual production reduced by Ahp activity on saturation; and $k'_{enz} = \frac{k^{Kat}_{cat}[Cat]}{K^{Kat}_M}$ (only Cat follows linear kinetics)

The study is similar to the previous one and internal H_2O_2 concentration can be expressed as follows:

$$[H_2O_2] = \left([H_2O_2]_{out0} - \frac{k'_{prod}}{k'_{enz}}\right)\frac{k_{diff}}{k_{diff}+k'_{enz}}\left(e^{\lambda'_1 t} - e^{\lambda'_2 t}\right) + \frac{k'_{prod}}{k'_{enz}}$$

with the eigenvalue $\lambda_1 \approx -\frac{k'_{enz}}{(k'_{enz}+k_{diff})}k'_{diff}$ and $\lambda_2 \approx -(k'_{enz} + k_{diff})$

The maximum will be $[H_2O_2]_{\max} \approx \frac{k_{diff}[H_2O_2]_{out0}}{k_{diff}+k'_{enz}}$. With large concentrations of exogenous H_2O_2, $[H_2O_2]_{\max} \approx \frac{k_{diff}[H_2O_2]_{out0}}{k_{diff}+\frac{k^{Kat}_{cat}[Cat]}{K^{Kat}_M}}$. This corresponds to the ratio of the rate of H_2O_2 influx by diffusion to its elimination by Cat or by diffusion only.

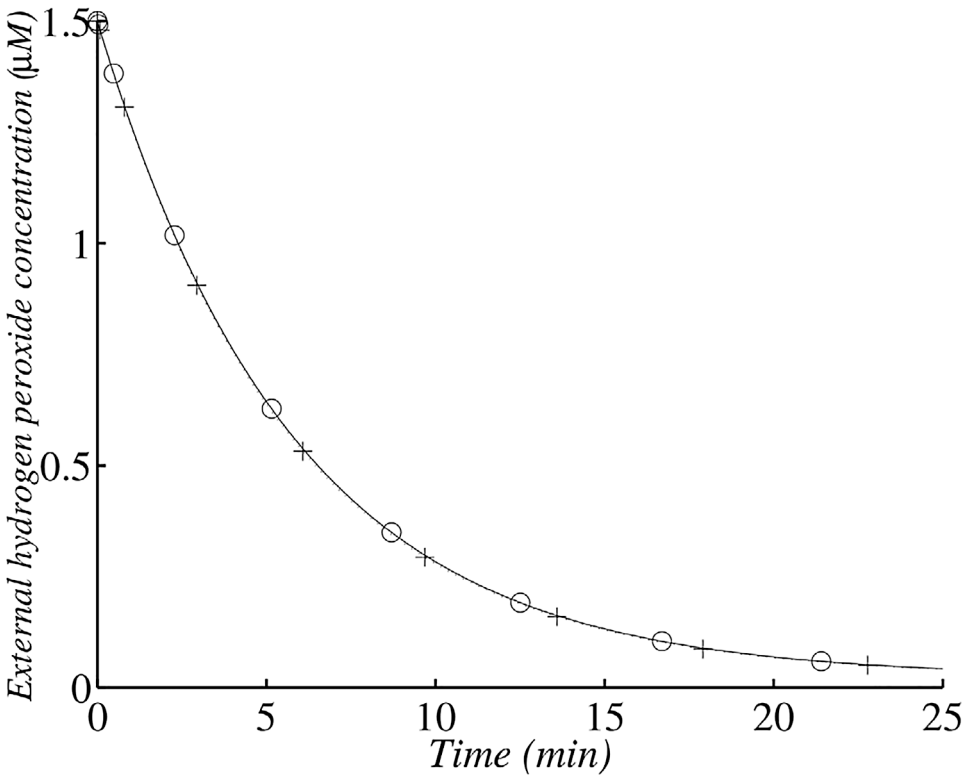

Fig 8. Changes in external H_2O_2 concentration in the wild type after the addition of 1.5 μM exogenous H_2O_2 with 1.45×10^7 cells ml^{-1}. (+) corresponds to the analytical solution according to the simplified system and (○)) corresponds to the numerical solution of the whole model. The simulation was run with 1.45×10^7 cells ml^{-1} (corresponding to an OD_{680} value of 0.1).

doi:10.1371/journal.pone.0159706.g008

This expression shows that the ratio between the initial exogenous H_2O_2 concentration and the maximal internal H_2O_2 concentration in the cell is:

$$\frac{[H_2O_2]\,\max}{[H_2O_2]_{out0}} \approx \frac{1}{1+\frac{k_{cat}^{Kat}[Cat]}{k_{diff}K_M^{Kat}}} \approx \frac{1}{2.2}\,(*)$$

The contribution of each elimination process to the value of the maximal internal H_2O_2 concentration is:

$$\frac{k'_{enz}}{k'_{enz}+k_{diff}} \approx 55\%\ \text{to Cat}$$

$$\text{and}\ \frac{k_{diff}}{k'_{enz}+k_{diff}} \approx 45\,\%\ \text{to elimination by diffusion across the cell membrane}$$

We notice that: $\frac{[H_2O_2]\,\max}{[H_2O_2]_{out0}}$ is equal to the ratio of elimination by diffusion across the membrane to the sum diffusion and scavenging. Of course, without membrane this ratio will equal 1, so thanks to membrane, enzymes have to face less H_2O_2. Moreover, at high exogenous H_2O_2 concentrations, this ratio is quite different from the one (i.e. 1/9) obtained at low concentration.

For instance, with an initial H_2O_2 exogenous concentration $[H_2O_2]_{out0} = 1$ mM, we obtain $[H_2O_2]_{\max} \approx 0.45$ mM (Fig 10). The maximal value is lower than the exogenous concentration

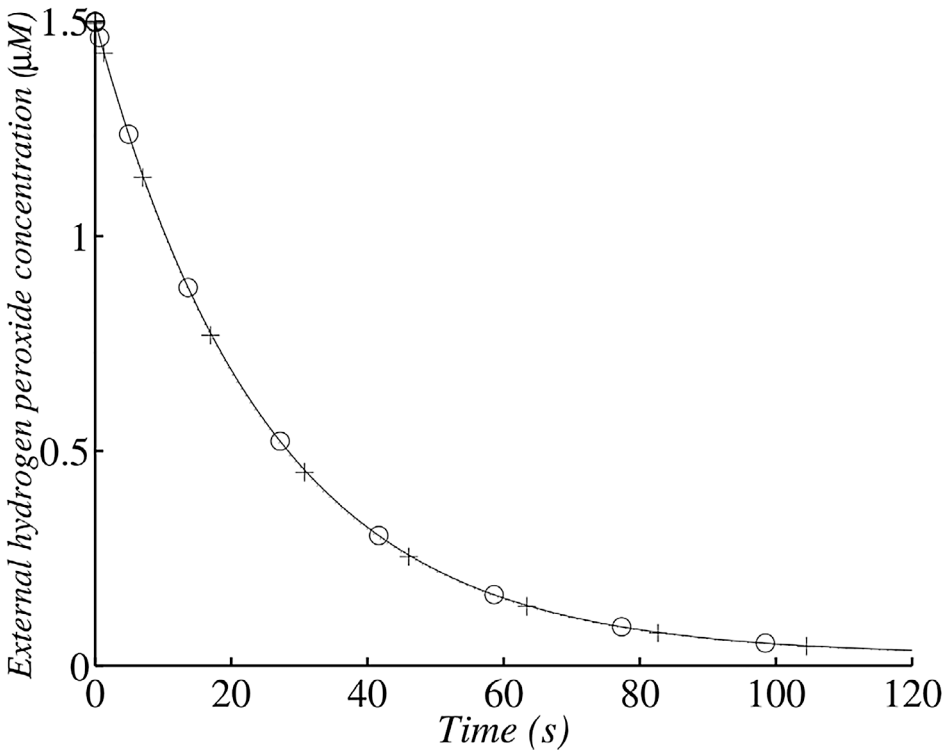

Fig 9. Changes in external H_2O_2 concentration in the wild type after the addition of 1.5 μM exogenous H_2O_2 with 2×10^8 cells ml^{-1}. (+) corresponds to the analytical solution according to the simplified system and (○)) corresponds to the numerical solution of the whole model. The simulation was run with 2×10^8 cells ml^{-1} (corresponding to an OD_{680} value of 0.1).

doi:10.1371/journal.pone.0159706.g009

because of diffusion and Cat activity, in this case Ahp is saturated and therefore plays a less important role.

The exogenous H_2O_2 concentration approximately follows the law outlined below:

$$[H_2O_2]_{out} = \left([H_2O_2]_0 - \frac{k_{prod}}{k_{enz}}\right) e^{\lambda'_1 t} + \frac{k_{prod}}{k_{enz}}$$

where

$$\lambda'_1 \approx -\frac{k'_{enz}}{(k'_{enz} + k_{diff})} k'_{diff} \neq k'_{diff}$$

This exponential decrease depends on λ'_1, which is a cell density function. The decrease rate of H_2O_2 can be characterized by the half-time $t_{1/2}$. This time is approximately the same for internal and external concentration, as internal and external H_2O_2 decrease are strongly linked. For instance, with an addition of 1 mM of exogenous H_2O_2 and with a cell density of 1.45×10^7 cells ml^{-1}, the half-live is approximately $t_{1/2} \approx \frac{\ln 1/2}{\lambda'_1} \approx 6.5$ minutes, this results is consistent with Fig 10.

Moreover, as the exponential decrease in rate is dependent on λ'_1, it ranges from zero when there is no scavenger (in a cat- mutant) to k'_{diff} when scavengers have a non-limiting rate constant (much higher than k_{diff}). Thus, a 10-fold induction of Cat (experimentally observed in an

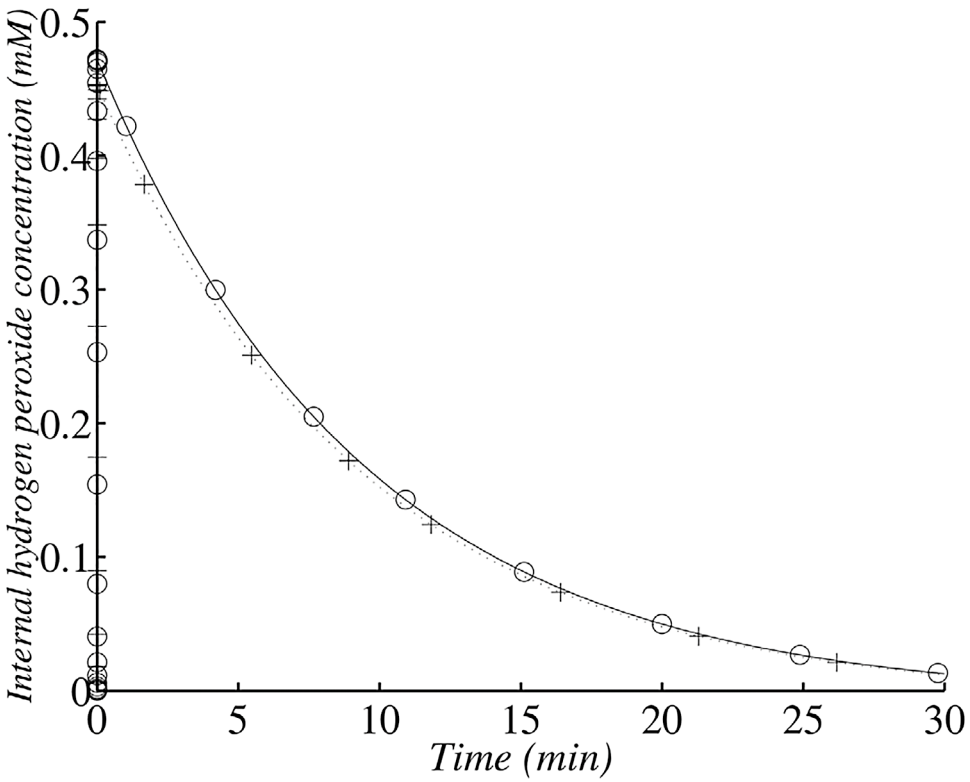

Fig 10. Changes in internal H_2O_2 concentration in the wild type after the addition of 1 mM exogenous H_2O_2 with 1.45 × 10^7 cells ml^{-1}. (+) corresponds to the analytical solution according to the simplified system and (○)) corresponds to the numerical solution of the whole model.

doi:10.1371/journal.pone.0159706.g010

Ahp(-) mutant) should increase the rate of medium detoxification of high H_2O_2 concentrations only with a ratio of:

$$\frac{\lambda'_{1,induction}}{\lambda'_1} = \lambda'_1 \approx \frac{10(k'_{enz} + k_{diff})}{(10k'_{enz} + k_{diff})} \approx 1.7$$

This result is consistent with the experimental data of Seaver and Imlay ([5]), who examined a doubling in efficiency when comparing the wild type and an Ahp(-) mutant.

It should also be noted that, in a Cat(-) mutant $[H_2O_2]_{\max} \approx [H_2O_2]_{out0} \approx [H_2O_2]_0$ (according to equation *). The maximum internal H_2O_2 concentration rapidly increases the exogenous H_2O_2 concentration and, as there is no Cat, this value remains constant, resulting in the rapid death of the surviving bacteria. The only way to protect Cat(-) mutant cells against high exogenous H_2O_2 concentrations is to add the wild type to the medium. This experiment has been reported by Ma and Eaton ([20]). This point will be examined in the following subsection.

Consequence of defence switch in the primary scavenger

Fig 11 shows that increasing exogenous H_2O_2 concentration involves the switch between the two primary scavengers. This switch has already been reported by Seaver and Imlay ([5]), but we show here another consequence. Actually this switch also triggers a change in the maximal internal H_2O_2 concentration viewed by cell. We also find that this maximal internal

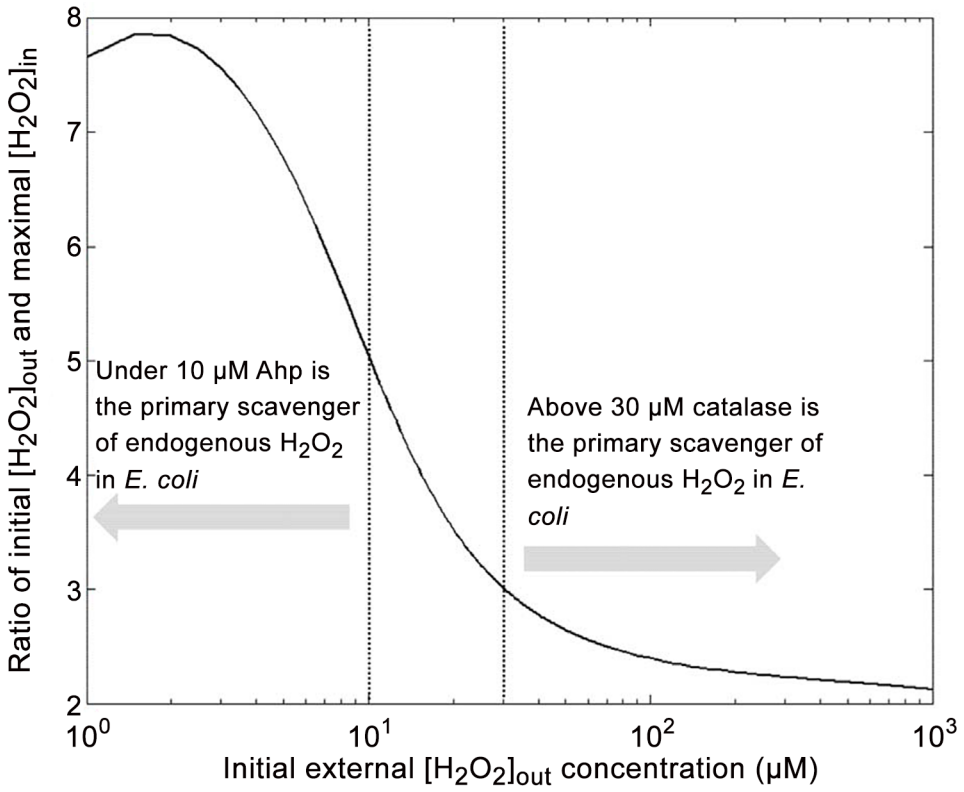

Fig 11. Changes in the ration between external initial H_2O_2 concentration and internal maximal H_2O_2 concentration in *E. coli* wild type. The numerical solution presented in this graph was running according to the whole model without approximation.

doi:10.1371/journal.pone.0159706.g011

concentration does not depend on the cell density. Nevertheless the temporal internal or external H_2O_2 decrease strongly depends on cell density (as previously reported in Figs 7 and 8 or in the previous subsection). The switch between the two scavengers also occurs in Fig 12, actually it shows that H_2O_2 half-life increases when shifting from Ahp to Cat while exogenous H_2O_2 increases.

This switch involves non-linear behaviour in half-life external H_2O_2 dependence. Once again, Ahp seems to be more efficient but it only concerns external H_2O_2 concentration under 10 μM. Above 30 μM, Cat plays the major role. Unlike maximal internal H_2O_2, half-life depends on cell density, and the more concentrated cells are, the faster medium detoxification occurs. Nevertheless, as reported in Fig 13, under 10 μM (Ahp is the primary scavenger) the half-life does almost not depend on the initial exogenous H_2O_2 concentration. Above 50 μM, Cat is the primary scavenger and the half-life depends on the initial exogenous H_2O_2 concentration.

Cumulative internal H_2O_2 concentration, rather than maximum internal H_2O_2 concentration, is involved in the H_2O_2-mediated death of bacterial cells. We investigated whether the decrease in *E. coli* survival with increasing exogenous H_2O_2 concentration was linked to theoretical maximum internal H_2O_2 concentration or to the rate of decrease in internal H_2O_2 concentration. Indeed, a steep decrease indicates the perception of a low mean internal H_2O_2 concentration by the cell. We investigated this aspect by carrying out experiments in which

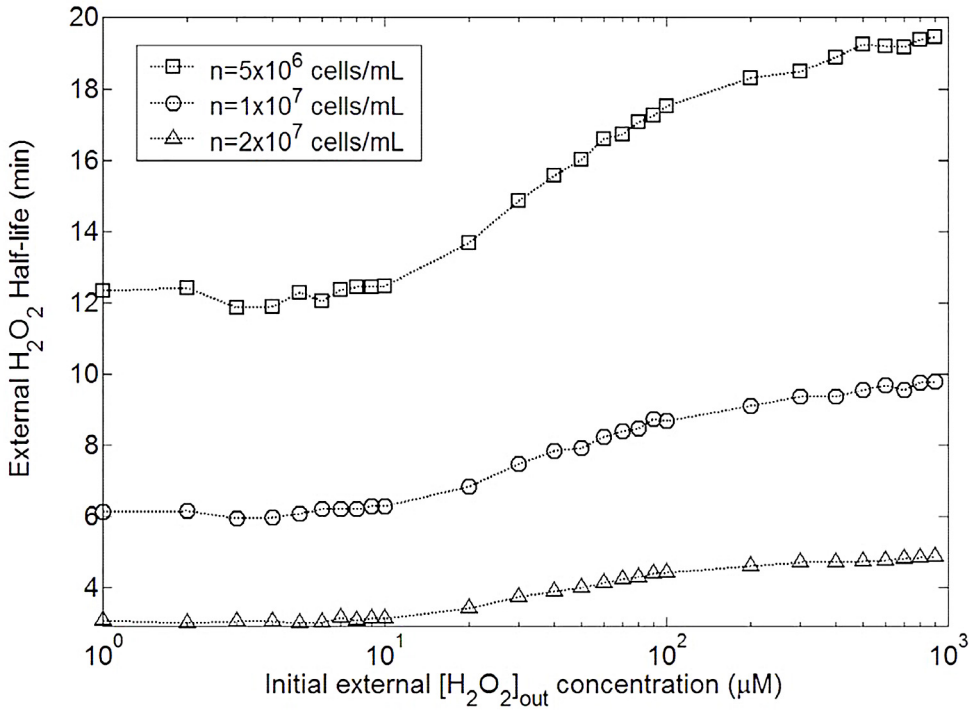

Fig 12. Changes in external H_2O_2 half-life with different initial external H_2O_2 concentrations and 3 different cell densities in *E. coli* wild type. The numerical solution presented in this graph was running according to the whole model without approximation.

doi:10.1371/journal.pone.0159706.g012

only one of these two parameters was affected at any one time. We therefore reproduced *in silico* the experiments of Ma and Eaton on H_2O_2-mediated killing by *E. coli* wild-type (Cat(+)) or Cat(-) strains alone or by cultures of *E. coli* containing similar numbers of Cat(+) and Cat(-) bacteria. Cat(-) cells from cultures of Cat(-) cells alone or from equal numbers of Cat(-) and Cat(+) cells had similar peak H_2O_2 concentrations but different rates of decrease in internal H_2O_2 concentration. This result led us to evaluate the involvement of these two parameters. Moreover, as these experiments were performed with diluted and concentrated cell cultures, giving similar peak H_2O_2 concentrations but different rates of decrease in internal H_2O_2 concentration, we also assessed the effect of these two parameters on cell death.

Simulations were performed with a dilute cell suspension (5×10^2 cells ml^{-1}, Figs 14 and 15) and a higher density of cells (10^7 cells ml^{-1}). Dilute populations of Cat(-) cells were unable to decrease exogenous H_2O_2 concentration. Dilute populations of Cat(+) cells were also unable to detoxify the medium (Fig 14), whereas the dense population of Cat(+) cells halved exogenous H_2O_2 concentration within 10 minutes (Fig 14). In a Cat(-) mutant, the maximum internal concentration of H_2O_2 was only 2.5 times higher than that in Cat(+) cells, but survival rates were similar for dilute populations of both Cat(-) and Cat(+) cells ([20]). As a conclusion, the maximum internal concentration of H_2O_2 is not a biological significant factor determining survival rate. Each single cell of the separate Cat(-) and Cat(+) populations had a maximum internal H_2O_2 concentration of about the same magnitude, but only cells from the high-density populations survived in the Eaton experiments. Survival rate was always high when medium detoxification was activated rapidly by a dense Cat(+) cell population. Thus, even Cat(-) *E. coli* can survive if they are mixed with Cat(+) cells able to detoxify the medium. We conclude that

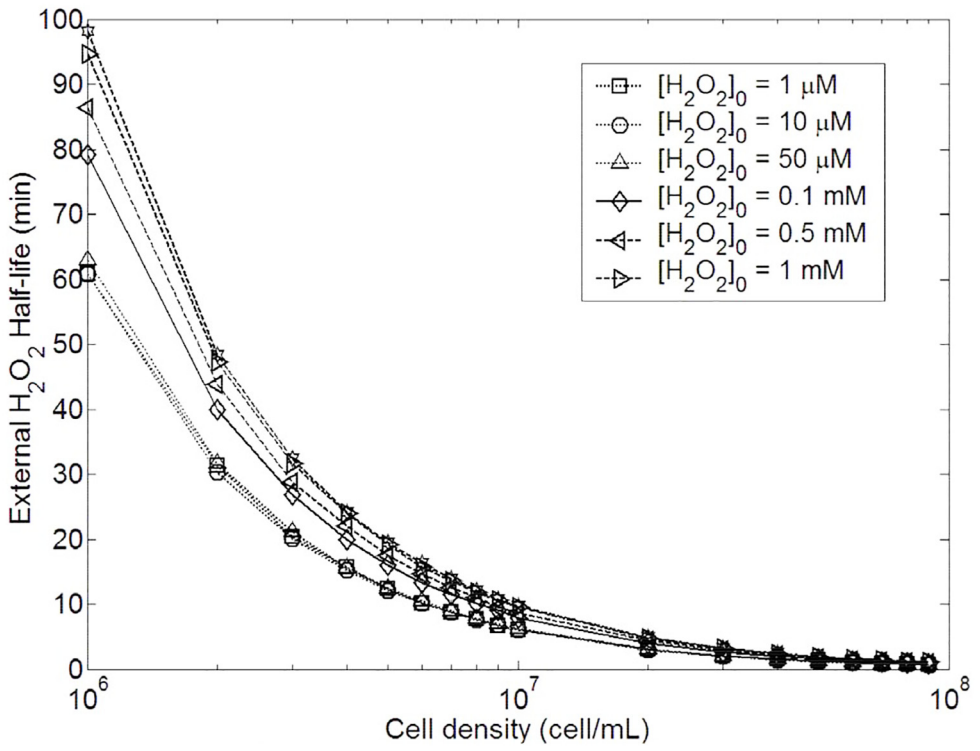

Fig 13. Changes in external H_2O_2 half-life with cell densities and with 7 different initial external H_2O_2 concentrations in *E. coli* wild type. The numerical solution presented in this graph was running according to the whole model without approximation.

doi:10.1371/journal.pone.0159706.g013

H_2O_2 scavengers do not protect individual cells against bulk-phase H_2O_2, because the maximum internal concentration of H_2O_2 did not differ significantly between Cat(-) and Cat(+) cells. The major difference between these two types of cells concerned the rate of decrease in exogenous H_2O_2 concentration and, consequently, the rate of decrease in internal H_2O_2 concentration (Fig 15). We conclude that mean internal H_2O_2 concentration has a significant impact on bacterial survival, whereas maximum internal H_2O_2 concentration does not. So H_2O_2 action can be compared to that of the radiative exposure. This means of action is the opposite of the one generally observed for drugs. For instance, the maximum amount of paracetamol for adults is 4 grams per day with a regular intake of 0.5 gram over 3 days, but a single intake of 10 grams can lead to liver failure ([21]).

Conclusions

In the absence of exogenous stress

An analysis of the most significant kinetic reactions confirmed that steady-state internal concentration H_2O_2 results from the balance between its production and a combination of Ahp degradation (78%), Cat degradation (12%) and membrane permeability (10%)

With exogenous H_2O_2 stress

Prediction of H_2O_2 levels. Under conditions of exogenous H_2O_2 stress, H_2O_2 elimination is dependent on cell density. However, nothing is currently known about internal H_2O_2

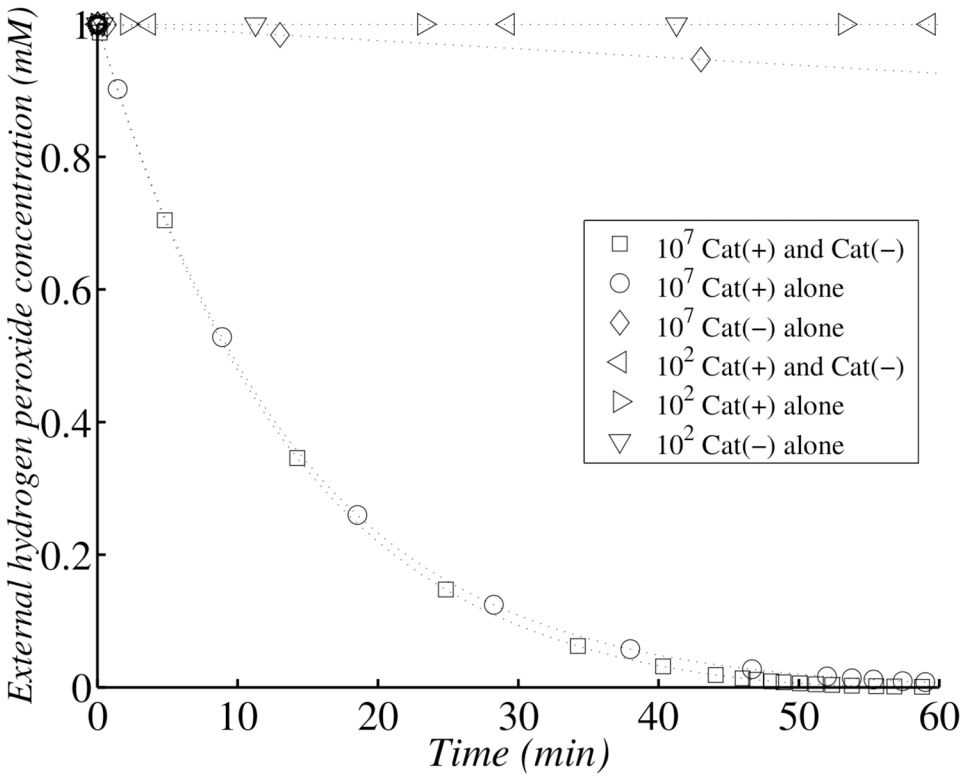

Fig 14. Simulation of Ma and Eaton experiment following external hydrogen peroxide concentration. Simulation of H_2O_2 external concentration change with dilute (10^2 cells per ml) Cat(-) *E. coli* alone (▽) or Cat (+) *E. coli* alone (▷) or admixed with an equal number of Cat(+), Cat(-) *E. coli* (◁); and with concentrated (10^7 cells per ml) Cat(-) *E. coli* alone (◇) or Cat(+) *E. coli* alone (○) or admixed with an equal number of Cat(+), Cat (-) *E. coli* (□). At zero time, H_2O_2 was added to a final concentration of 1.0 mM, and the bacterial suspension was then incubated at 37°C.

doi:10.1371/journal.pone.0159706.g014

concentration during H_2O_2 exposure. Under these conditions, internal H_2O_2 concentration results mostly from influx due to diffusion across the cell membrane, because endogenous production is negligible. Moreover, the rate of diffusion into the cell is governed by membrane permeability. The internal concentration of H_2O_2 must therefore be lower than the exogenous H_2O_2 concentration. Consequently, exogenous H_2O_2 stress leads to an increase in internal H_2O_2 concentration until a maximum is reached. This peak is followed by a decrease in H_2O_2 concentration, due to elimination by the cells. We aimed to identify the most significant parameters (kinetic constants and cell concentrations) accounting for the maximum internal H_2O_2 concentration value reached and for the characteristic time points (time required to reach half the nearest steady–state concentration) during increases and decreases in internal H_2O_2 concentration.

Surprisingly, based on our model, the maximal internal H_2O_2 concentrations reached in individual cells was not dependent on cell density, suggesting that there is no population protection effect. This maximum, which is reached in a few milliseconds, and its characteristic timing, are dependent solely on exogenous H_2O_2 concentration and the three routes of elimination of this radical (membrane permeability, Ahp and Cat scavenging).

For estimation of the maximal internal H_2O_2 concentration, we needed to distinguish internal H_2O_2 concentrations for which Ahp activity predominated from those for which Cat

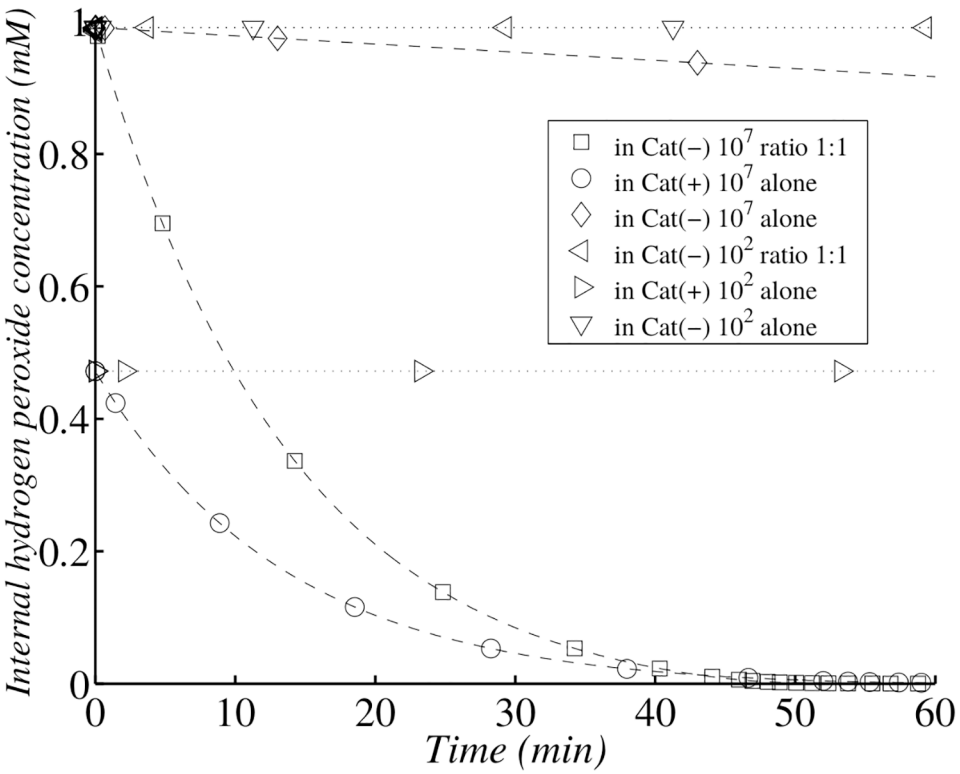

Fig 15. Simulation of Ma and Eaton experiment following internal hydrogen peroxide concentration. Simulation of H_2O_2 internal concentration change with dilute (10^2 cells per ml) Cat(-) *E. coli* alone (▽) or Cat (+) *E. coli* alone (⊳) or admixed with equal numbers of Cat(+), Cat(-) *E. coli* (◁); and with concentrated (10^7 cells per ml) Cat(-) *E. coli* alone (◇) or Cat(+) *E. coli* alone (○) or admixed with equal numbers of Cat(+), Cat(-) *E. coli* (□). At zero time, H_2O_2 was added to a final concentration of 1.0 mM, and the bacterial suspension was then incubated at 37°C.

doi:10.1371/journal.pone.0159706.g015

activity predominated. For initial exogenous H_2O_2 concentrations below 10 μM, the maximal internal H_2O_2 concentration was defined by the balance between the exogenous H_2O_2 diffusion rate and the three routes of elimination. In these conditions, Ahp was responsible for about 78% of all the H_2O_2 eliminated. The peak internal H_2O_2 concentration was almost one tenth the concomitant exogenous H_2O_2 concentration. At initial exogenous H_2O_2 concentrations of more than 30 μM, the peak internal H_2O_2 concentration was defined by the balance between the exogenous H_2O_2 diffusion rate and the possible elimination routes (Ahp activity being negligible due to saturation). Thus, peak H_2O_2 concentrations are determined not only by Cat activity (55%), but also by membrane permeability (45%). Surprisingly, at the peak internal H_2O_2 concentration sensed by each cell, limited membrane permeability served as a passive defence against H_2O_2, to a similar extent to Cat. In these conditions, internal H_2O_2 concentration was only half the concomitant exogenous H_2O_2 concentration.

We then showed that the rate of decrease in internal H_2O_2 concentration and its characteristic timing were dependent principally on cell density and membrane permeability. This decrease was mediated not only by enzyme activity, but also by H_2O_2 transport from the extracellular to the intracellular medium. The global kinetics of the decrease in internal H_2O_2 concentration was determined by the slowest step in the process, diffusion across the membrane, which was limited by cell membrane permeability. Finally, similar conclusions were reported

for exogenous H_2O_2 concentration. The Imlay group has shown that the elimination rate for exogenous H_2O_2 is much lower in intact cells than in cell extracts, indicating that diffusion across the cell membrane is the limiting process. This observation is consistent with what is known about the most significant kinetic parameters, including the major role played by the cell membrane. Indeed, diffusion across the cell membrane involves the bridging of a gap between internal and extracellular concentrations. This gap provides protection against the oxidizing extracellular medium, but it also decreases the efficiency with which *E. coli* can decrease the H_2O_2 concentration of the extracellular medium (Fig 9). The kinetics of extracellular decomposition is almost exclusively diffusion-dependent and, therefore, very slow. As expected, the rate of H_2O_2 disappearance (intra or extracellular) was greater at higher cell densities.

Instead of conducting real-world experiments, using simulations is generally cheaper, safer and sometimes more ethical. Simulations can also be conducted faster than experiments in real time. For instance, at the University of Pittsburgh School of Pharmacy, high-fidelity patient simulators are used in addition to therapeutics ([22]). Of course simulations have to be confronted with real experiments to test their robustness and to be improved. Our model is one step in a global modelling of the *E. coli* ROS dynamic.

"Remember that all models are wrong; the practical question is how wrong do they have to be to not be useful."

— Box and Draper, Empirical Model-Building, p. 74

Supporting Information

S1 File. Superoxide kinetic and evolution.
(PDF)

Acknowledgments

Our thanks go to A. Dumont, E. Fugier, P. Caillet and K. Wilson-Costa for carefully proof the manuscript.

Author Contributions

Conceived and designed the experiments: LU SD.

Performed the experiments: LU SD.

Analyzed the data: LU SD.

Contributed reagents/materials/analysis tools: LU SD.

Wrote the paper: LU SD.

References

1. Barry Halliwell, John M C Gutteridge. Free radicals in biology and medicine. Clarendon Press; 1989.
2. Kehrer JP. Free radicals as mediators of tissue injury and disease. Crit Rev Toxicol. 1993; 23(1):21–48. doi: 10.3109/10408449309104073 PMID: 8471159
3. Uhl L, Gerstel A, Chabalier M, Dukan S. Hydrogen peroxide induced cell death: One or two modes of action? Heliyon. 2015; 1(4):Article e00049 doi: 10.1016/j.heliyon.2015.e00049 PMID: 27441232
4. Seaver LC, Imlay JA. Hydrogen peroxide fluxes and compartmentalization inside growing Escherichia coli. J Bacteriol. 2001 Dec; 183(24):7182–7189. doi: 10.1128/JB.183.24.7182-7189.2001 PMID: 11717277

5. Seaver LC, Imlay JA. Alkyl hydroperoxide reductase is the primary scavenger of endogenous hydrogen peroxide in Escherichia coli. J Bacteriol. 2001 Dec; 183(24):7173–7181. doi: 10.1128/JB.183.24.7173-7181.2001 PMID: 11717276
6. Imlay JA, Linn S. Bimodal pattern of killing of DNA-repair-defective or anoxically grown Escherichia coli by hydrogen peroxide. J Bacteriol. 1986 May; 166(2):519–527. PMID: 3516975
7. Imlay JA, Linn S. DNA damage and oxygen radical toxicity. Science. 1988 Jun; 240(4857):1302–1309. doi: 10.1126/science.3287616 PMID: 3287616
8. Harrison J, Leggett R, Lloyd D, Phipps A, Scott B. Polonium-210 as a poison. J Radiol Prot. 2007 Mar; 27(1):17–40. doi: 10.1088/0952-4746/27/1/001 PMID: 17341802
9. Gillespie DT. A general method for numerically simulating the stochastic time evolution of coupled chemical reactions. Journal of Computational Physics. 1976; 22(4):403–434. doi: 10.1016/0021-9991(76)90041-3
10. Gillespie DT. Exact stochastic simulation of coupled chemical reactions. J Phys Chem. 1977; 81 (22):2340–2361. doi: 10.1021/j100540a008
11. Koppenol WH. The Haber-Weiss cycle–70 years later. Redox Rep. 2001; 6(4):229–234. doi: 10.1179/135100001101536373 PMID: 11642713
12. Liochev SI, Fridovich I. The Haber-Weiss cycle–70 years later: an alternative view. Redox Rep. 2002; 7 (1):55–57. doi: 10.1179/135100002125000190 PMID: 11981456
13. Verhulst PF. Recherches mathématiques sur la loi d'accroissement de la population. Nouv mém de l'Academie Royale des Sci et Belles-Lettres de Bruxelles. 1845; 18:1–41.
14. Verhulst PF. Deuxième mémoire sur la loi d'accroissement de la population. Mém de l'Académie Royale des Sci, des Lettres et des Beaux-Arts de Belgique. 1847; 20:1–32.
15. Demple B, Halbrook J. Inducible repair of oxidative DNA damage in Escherichia coli. Nature. 1983; 304 (5925):466–468. doi: 10.1038/304466a0 PMID: 6348554
16. Chang DE, Smalley DJ, Conway T. Gene expression profiling of Escherichia coli growth transitions: an expanded stringent response model. Mol Microbiol. 2002 Jul; 45(2):289–306. doi: 10.1046/j.1365-2958.2002.03001.x PMID: 12123445
17. Imlay JA, Fridovich I. Assay of metabolic superoxide production in Escherichia coli. J Biol Chem. 1991 Apr; 266(11):6957–6965. PMID: 1849898
18. Polynikis A, Hogan SJ, di Bernardo M. Comparing different ODE modelling approaches for gene regulatory networks. J Theor Biol. 2009 Dec; 261(4):511–530. doi: 10.1016/j.jtbi.2009.07.040 PMID: 19665034
19. Gonzalez-Flecha B, Demple B. Metabolic sources of hydrogen peroxide in aerobically growing Escherichia coli. J Biol Chem. 1995 Jun; 270(23):13681–13687. doi: 10.1074/jbc.270.23.13681 PMID: 7775420
20. Ma M, Eaton JW. Multicellular oxidant defense in unicellular organisms. Proc Natl Acad Sci USA. 1992 Sep; 89(17):7924–7928. doi: 10.1073/pnas.89.17.7924 PMID: 1518815
21. Dart RC, Erdman AR, Olson KR, Christianson G, Manoguerra AS, Chyka PA, et al. Acetaminophen poisoning: an evidence-based consensus guideline for out-of-hospital management. Clin Toxicol (Phila). 2006; 44(1):1–18. doi: 10.1080/15563650500394571
22. Lin K, Travlos DV, Wadelin JW, Vlasses PH. Simulation and introductory pharmacy practice experiences. Am J Pharm Educ. 2011 Dec; 75(10):209. doi: 10.5688/ajpe7510209 PMID: 22345728